Geophysical Research Letters

RESEARCH LETTER
10.1029/2020GL089202

Quantitatively Tracking the Elevation of the Tibetan Plateau Since the Cretaceous: Insights From Whole-Rock Sr/Y and La/Yb Ratios

Fangyang Hu[1,2], Fuyuan Wu[1,3,4], James B. Chapman[5], Mihai N. Ducea[2,6], Weiqiang Ji[1,4], and Shuwen Liu[7]

[1]State Key Laboratory of Lithospheric Evolution, Institute of Geology and Geophysics, Chinese Academy of Sciences, Beijing, China, [2]Department of Geosciences, University of Arizona, Tucson, AZ, USA, [3]College of Earth and Planetary Sciences, University of Chinese Academy of Sciences, Beijing, China, [4]Innovation Academy for Earth Science, Chinese Academy of Sciences, Beijing, China, [5]Department of Geology and Geophysics, University of Wyoming, Laramie, WY, USA, [6]Faculty of Geology and Geophysics, University of Bucharest, Bucharest, Romania, [7]Key Laboratory of Orogenic Belts and Crustal Evolution, Ministry of Education, School of Earth and Space Sciences, Peking University, Beijing, China

Abstract Crustal thickness, elevation, and Sr/Y and $(La/Yb)_N$ of magmatic rocks are strongly correlated for subduction-related and collision-related mountain belts. We quantitatively constrain the paleo-elevation of the Tibetan Plateau since the Cretaceous using empirically derived equations. The results are broadly consistent with previous estimates based on stable isotope and structural analyses, supporting a complex uplift history. Our data suggest that a protoplateau formed in central Tibet during the Late Cretaceous and was higher than the contemporaneous Gangdese arc. This protoplateau collapsed before the India-Asia collision, during the same time period that elevation in southern Tibet was increasing. During the India-Asia collision, northern and southern Tibet were uplifted first followed by renewed uplift in central Tibet, which suggests a more complicated uplift history than commonly believed. We contend that a broad paleovalley formed during the Paleogene in central Tibet and that the whole Tibetan Plateau reached present-day elevations during the Miocene.

Plain Language Summary Paleo-elevation is an important factor in understanding the mountain building processes. Strong correlations are observed between crustal thickness, elevation, and Sr/Y and $(La/Yb)_N$ of magmatic rocks for both subduction-related and collision-related mountain belts. We established empirical equations derived from modern examples and applied them to constrain the paleo-elevation evolution of the Tibetan Plateau since the Cretaceous. Our calculated results are broadly consistent with previous estimates based on stable isotope and structural analyses and document a complex uplift history. In central Tibet, a proto-plateau with an elevation >3,000 m was formed during the Late Cretaceous and was higher than the Gangdese continental arc in the south. This protoplateau collapsed at the same time as the southern Tibet plateau (Lhasaplano) was uplifted prior to the India-Asia collision formed before the India-Asia collision. During the India-Asia collision in the Cenozoic, northern and southern Tibet were uplift first, followed by uplift of central Tibet. A paleovalley was formed in central Tibet during the Paleogene and elevations of the whole Tibetan Plateau similar to the present-day were achieved during the Miocene.

Key Points:
- Sr/Y and $(La/Yb)_N$ ratios of magmatic rocks can be used for estimating paleo-elevation of orogenic belts
- Two protoplateaus were formed successively during the Late Cretaceous in the central and southern Tibet before India-Asia collision
- A paleovalley formed during the Paleogene in central Tibet and the Tibetan Plateau reached present-day elevations during the Miocene

Supporting Information:
- Supporting Information S1

Correspondence to:
F. Hu,
hufangyang@mail.iggcas.ac.cn

Citation:
Hu, F., Wu, F., Chapman, J. B., Ducea, M. N., Ji, W., & Liu, S. (2020). Quantitatively tracking the elevation of the Tibetan Plateau since the cretaceous: Insights from whole-rock Sr/Y and La/Yb ratios. *Geophysical Research Letters*, *47*, e2020GL089202. https://doi.org/10.1029/2020GL089202

Received 10 JUN 2020
Accepted 13 JUL 2020
Accepted article online 19 JUL 2020

1. Introduction

The paleo-elevation history of the Tibetan Plateau (TP) remains a topic of intense debate (Botsyun et al., 2019; Deng et al., 2012, 2019; Deng & Ding, 2015; Ding et al., 2014, 2017; Ingalls et al., 2018; Quade et al., 2011; Rowley & Currie, 2006; Rowley & Garzione, 2007; Spicer et al., 2003; Su et al., 2019; Sun, Wang, et al., 2015; Xu et al., 2013). Stable isotope (including clumped-isotope) studies proposed that the majority of the TP reached its present elevation during the Eocene (e.g., Ding et al., 2014; Ingalls et al., 2018; Rowley & Currie, 2006). However, paleontological studies questioned this viewpoint, suggesting that the TP did not achieve its present elevation until the Miocene (e.g., Deng et al., 2019; Deng & Ding, 2015; Su et al., 2019). Several models have been proposed for the Cenozoic uplift history of the TP, including synchronous uplift, northward stepwise uplift, incremental northward uplift, and differential uplift (England & Houseman,

1989; Law & Allen, 2020; Liu et al., 2016; Tapponnier et al., 2001). The pre-Cenozoic uplift history of the TP has only been described qualitatively and there is little information available outside of the Lhasa terrane (DeCelles et al., 2007; Kapp, DeCelles, Gehrels, et al., 2007; Lai, Hu, Garzanti, Sun, et al., 2019). The Gangdese arc region was thought to be at a relatively low elevation during the Early Cretaceous and become the Lhasaplano during the late Late Cretaceous to Paleocene (Ding et al., 2014; Kapp, DeCelles, Leier, et al., 2007). Another protoplateau (Northern Lhasaplano) was proposed to be formed in the Northern and Central Lhasa terranes with a width >160 km during the early Late Cretaceous (Lai, Hu, Garzanti, Sun, et al., 2019).

Most of the studies listed above use stable isotope (including clumped-isotope) or paleontological methods to estimate paleo-elevations (e.g., Currie et al., 2005; Deng et al., 2019; Ding et al., 2017; Ingalls et al., 2018; Quade et al., 2011; Rowley & Garzione, 2007; Spicer et al., 2003; Su et al., 2019). In recent years, additional methods have been developed to estimate Moho depth based on whole-rock geochemical and isotopic compositions of intermediate to felsic magmatic rocks (Alexander et al., 2019; Chapman et al., 2015; Chiaradia, 2015; Hu et al., 2017; Profeta et al., 2015), or the compositions of accessory minerals such as zircon (Balica et al., 2020; McKenzie et al., 2018). Since most convergent margins are in isostatic equilibrium at scales of hundreds of kilometers, there is a direct correlation between crustal thickness and elevation assuming crustal Airy equilibrium (Airy, 1855; Lee et al., 2015), described as

$$dh/dH = (1 - \rho_c/\rho_m) \quad (1)$$

where h is the elevation, H is the crustal thickness, ρ_c is the crustal density, and ρ_m is the upper mantle density. Zhu et al. (2017) have estimated paleo-elevation for the southern Tibet using a two-step processes where they first calculated paleo-Moho depths using the equations of Profeta et al. (2015) then related those depths to paleo-elevation assuming Airy isostatic equilibrium (Equation 1) with constant crustal and mantle densities. This contribution updates these previous studies by (1) directly establishing an empirical relation between elevation and Sr/Y and $(La/Yb)_N$ ratios of magmatic rocks, (2) exploring how variable crustal and mantle densities may affect paleo-elevation, and (3) expanding the analysis to central and northern Tibet. Reconstructing paleo-elevation changes for the TP since the Cretaceous suggests diachronous uplift and reveals a more dynamic uplift history than previously believed.

2. Methods

2.1. Empirical Correlation Equations

A global compilation of geochemical data of magmatic rocks from modern subduction zones and collisional zones and their corresponding elevations are presented in the Tables S1 and S2 in the supporting information. The data are organized into subsets based on location. Elevation for each data subset comes from the U.S. Geological Survey (USGS) National Elevation Dataset and National Aeronautics and Space Administration (NASA) Shuttle Radar Topography Mission and was averaged after smoothing. Elevation uncertainty (1σ) is based on the standard deviation of individual sample location elevations within the data subsets. Moho depth is calculated based on the CRUST 1.0 model (http://igppweb.ucsd.edu/~gabi/rem.html), and referenced from Chapman et al. (2015), Profeta et al. (2015), and Hu et al. (2017) (Tables S3 and S4). A weighted least squares regression between the elevation and Moho depth was established for subduction-related and collisional zones, respectively (Figure 1).

Geochemical data were filtered and processed using the methods of Chapman et al. (2015) and Hu et al. (2017) (Tables S3 and S4). Our data subsets include geochemical data from the Pliocene to Quaternary age magmatic rocks for both subduction and collision zones. Miocene geochemical data from the TP are also included in our database because the Miocene paleo-elevation data are well constrained and widely accepted (e.g., Currie et al., 2005; Quade et al., 2011; Rowley & Currie, 2006; Spicer et al., 2003). Samples from subduction zones with SiO_2 of 55–70 wt.%, MgO of 1.0–6.0 wt.%, and Rb/Sr ratio of 0.05–0.20 and samples from collision zones with SiO_2 of 55–72 wt.% and MgO of 0.5–6.0 wt.% were selected. These criteria were chosen to remove samples formed by partial melting, assimilation or fractional crystallization at shallow crustal levels, which will result in an underestimate of true crustal thickness (elevation) (Chapman et al., 2015; Hu et al., 2017). We then removed Sr/Y and $(La/Yb)_N$ outliers from each data subsets by using

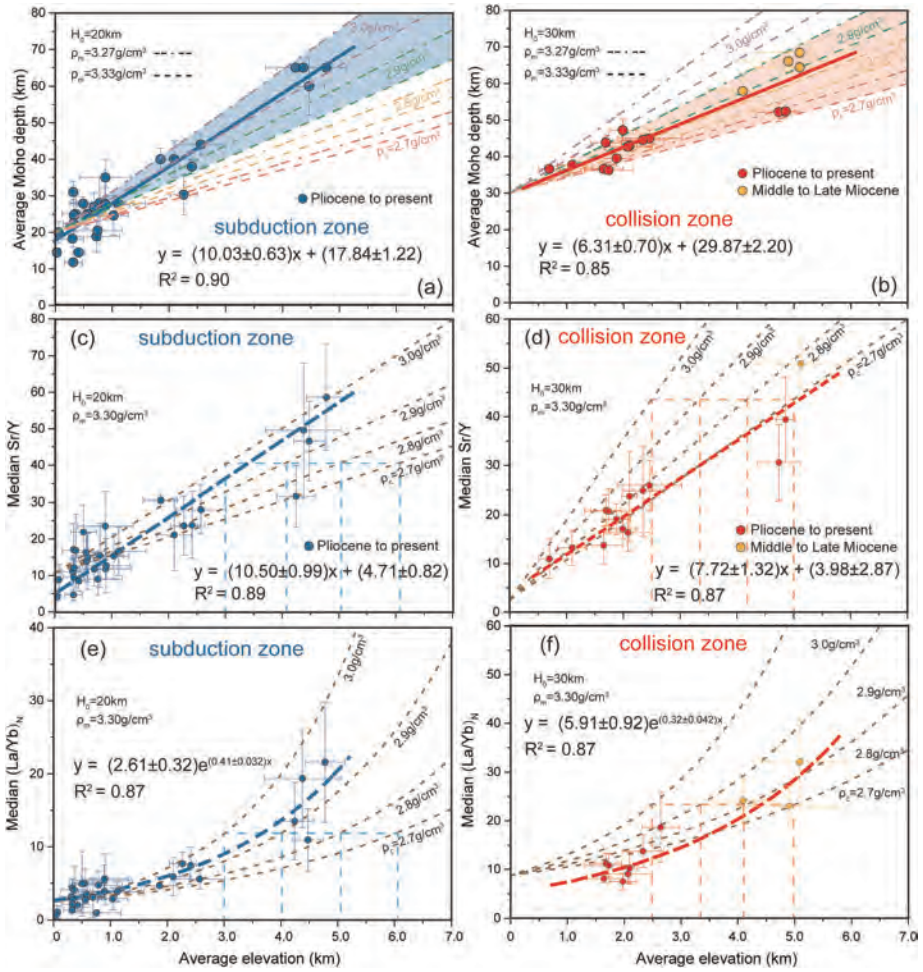

Figure 1. Global correlations between averaged elevations and average Moho depth, median Sr/Y and $(La/Yb)_N$ ratios from subduction zones (a, c, and e) and collision zones (b, d, and f). The blue circles represent the magmatic rocks from subduction zones formed during the Pliocene to present. The red (Pliocene to present) and orange circles (Middle to Late Miocene) represent magmatic rocks from collision zones. The brown dashed lines represent calculated reference lines based on the Airy isostasy and relationships between the Moho depth and median Sr/Y and $(La/Yb)_N$ (Chapman et al., 2015; Hu et al., 2017; Profeta et al., 2015). The given zero-elevation crustal thickness (H_0) and density of mantle (ρ_m) and crust (ρ_c) are shown on each diagram.

modified Thompson tau statistical method and calculated the median values of Sr/Y and $(La/Yb)_N$ and their standard deviations. We discarded data subsets with standard deviations higher than 10, except for those from the Andes. The data subsets from collision zones with average Rb/Sr higher than 0.35 were also rejected (Hu et al., 2017). The high La data subsets (>70 ppm) from collision zones were excluded from La/Yb compilation because the potential high temperature melting strongly elevates the La content but has little impact on Sr, Y, and Yb contents, which leads to extremely high La/Yb ratios and their failure to constrain elevation (Figure S1).

We performed a weighted least squares regression through these data subsets to obtain the correlation equations presented in Figure 1. Because we relate geochemical composition to elevation directly, no assumptions about variations in crustal and/or mantle densities are required. However, it is instructive to compare our empirically derived paleo-elevation equations to models that relate $(La/Yb)_N$ ratio to paleo-elevation assuming Airy isostacy (e.g., Zhu et al., 2017). We explore a range of crustal and upper mantle densities based on the range of published *P*/*S* wave velocities and layer thicknesses for modern subduction and collisional orogenic systems (Figure S2 and Table S5; Brocher, 2005). The transformation from *P*/*S*

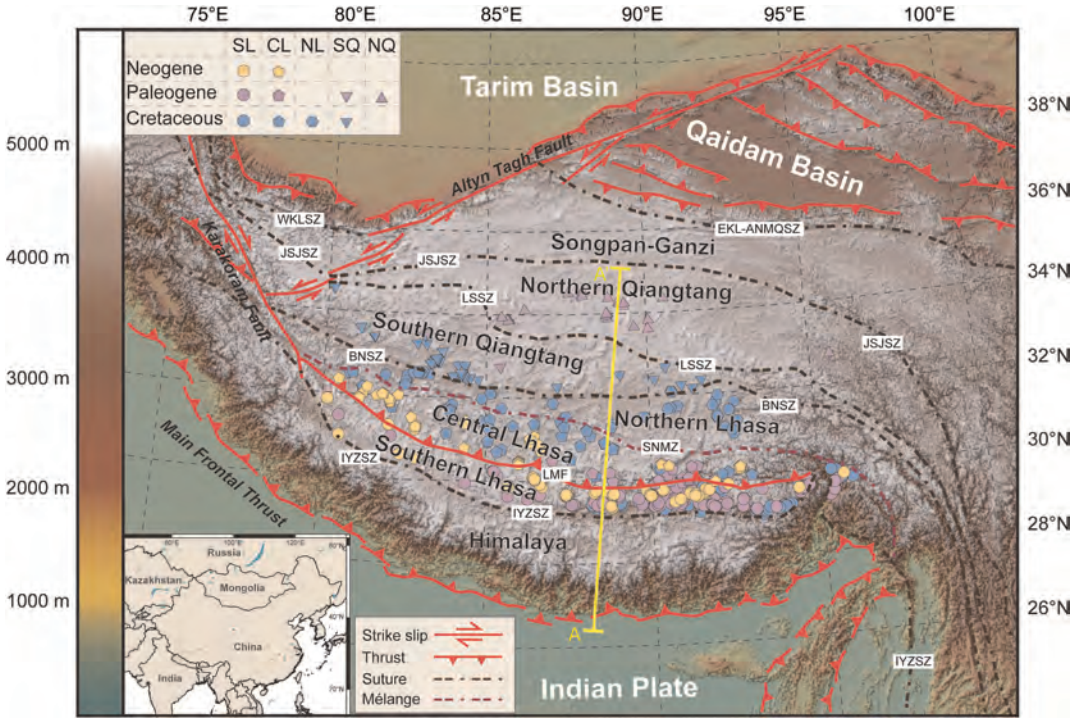

Figure 2. Digital elevation map of the TP showing the main active faults, suture zones, and terranes (after Taylor & Yin, 2009; Searle et al., 2016). The symbols represent locations and formation time of complied data. The abbreviations of main terranes are as follows: SL—Southern Lhasa; CL—Central Lhasa; NL—Northern Lhasa; SQ—Southern Qiangtang; NQ—Northern Qiangtang. The abbreviations of faults, mélange, and suture zones separating the main terranes are as follows: EKL-ANMQSZ—Eastern Kunlun-Animaqing suture zone; JSJSZ—Jinshajiang suture zone; LSSZ—Longmuco-Shuanghu suture zone; BNSZ—Bangong-Nujiang suture zone; SNMZ—Shiquanhe-Nam Tso mélange zone; LMF—Luobadui-Milashan fault; IYZSZ—Indus-Yarlung Zangbo suture zone.

wave velocity to crustal density is based on the Nafe-Drake curve (Equation 2) and Brocher's regression fit (Equation 3) (Brocher, 2005), described as

$$\rho\ (\mathrm{g/cm^3}) = 1.6612V_P - 0.4721V_P^2 + 0.0671V_P^3 - 0.0043V_P^4 + 0.000106V_P^5 \quad (2)$$

$$V_P\ (\mathrm{km/s}) = 0.9409 + 2.0947V_S - 0.8206V_S^2 + 0.2683V_S^3 - 0.0251V_S^4 \quad (3)$$

where ρ is the crustal density, V_p is the P wave velocity, and V_s is the S wave velocity. The upper mantle density refers to the values provided by He et al. (2014) and Lee et al. (2015).

2.2. The Tibetan Plateau

Geochemical data for Cretaceous to recent magmatic rocks in the TP were obtained from the Tibetan Magmatism Database (Table S6; Chapman & Kapp, 2017). Following previous authors (Yi et al., 2018; Zhu et al., 2019), we subdivided the Qiangtang and Lhasa terranes into five subterranes, including the Northern Qiangtang, Southern Qiangtang, Northern Lhasa, Central Lhasa, and Southern Lhasa terranes and investigate the paleo-elevation history of each separately (Figure 2). Because of the distinct tectonic settings of different terranes during different time periods, subduction-related and collision-related equations were applied for each terrane according to specific circumstances (see Table S7). Both methods were employed for comparison of magmatic rocks formed during the transition time form oceanic subduction to continental collision (e.g., ~65–45 Ma for the Central and Southern Lhasa terranes). Paleo-elevation uncertainty is reported at the 2σ level and includes the uncertainty from the equation used and the standard deviation of Sr/Y or $(La/Yb)_N$ of each data subset.

3. Results and Discussion

3.1. Empirical Equations and Their Limitation

The empirical equations between the median Sr/Y and $(La/Yb)_N$ ratios of magmatic rocks and average elevations from subduction and collision zones are shown in Figure 1. The calculated regressions show good correlations with $R^2 > 0.85$. The empirical equations for subduction zones are as follows:

$$Sr/Y_S = (10.50 \pm 0.99) \times E + (4.71 \pm 0.82) \quad (4)$$

$$\left[(La/Yb)_N\right]_S = (2.61 \pm 0.32)e^{(0.41 \pm 0.032)E} \quad (5)$$

where E is the elevation in meters and the subscript "S" means the subduction zone models. The empirical equations for collision zones are as follows:

$$Sr/Y_C = (7.72 \pm 1.32) \times E + (3.98 \pm 2.87) \quad (6)$$

$$\left[(La/Yb)_N\right]_C = (5.91 \pm 0.92)e^{(0.32 \pm 0.042)E} \quad (7)$$

where the subscript "C" refers to the collision zone models.

Based on the typical standard deviation of Sr/Y and $(La/Yb)_N$ in the data subsets and the uncertainty in our empirically derived equations, the average uncertainty of this method is 500 to 1,500 m (Figure S3). Paleo-elevation estimates higher than 6,000 m for subduction systems [$Sr/Y > 65$; $(La/Yb)_N > 30$] and collision zones [$Sr/Y > 50$; $(La/Yb)_N > 40$] and lower than 1,000 m [$(La/Yb)_N < 8$] for collision zones are not considered valid because this range of values are not constrained by the data used to create the empirical relationships.

Strong correlations ($R^2 > 0.85$) between the elevation and Moho depth in modern subduction and collision zones confirm the effectiveness of Equations 4–7 (Figure 1). The differences in equations for subduction zones and equations for collision zones are interpreted to be caused by the variations in crust and upper mantle density (Figure 1; Bassett et al., 2016; Lee et al., 2015). Previous studies that calculating paleo-elevation based on Airy isostasy and paleocrustal thickness (e.g., Chapman et al., 2020; Zhu et al., 2017) implicitly assume that the crust and upper mantle density have not changed, which may not be valid for ancient orogens. Figure 1 shows how using different densities of the crust and upper mantle could influence estimates of paleo-elevation. The data suggest that choosing incorrect density values could result in paleo-elevation estimates up to 3,000 m away from a true value (Figures 1 and S2). Therefore, our equations, which do not require assumption about density, could help reduce uncertainty. Figure 1 also makes predictions for the average crustal density in subduction and collisional systems based on our empirical equations, although this was not our primary goal. The predicted average crustal densities of ~2.8–3.0 g/cm^3 for subduction zones and ~2.6–2.8 g/cm^3 for collision zones are geologically realistic values and supports the utility of our new equations (Figure S2).

3.2. Paleo-Elevation in the Tibetan Plateau Since the Cretaceous

Our results are consistent with previous estimates based on stable isotopes (Figure 3; Tables S7 and S8; e.g., Currie et al., 2005; Ding et al., 2014; Ingalls et al., 2018; Xu et al., 2013). Results calculated from Sr/Y and $(La/Yb)_N$ generally overlap within uncertainty (Figure S4). When results calculated from both methods differ, the higher value was chosen to represent the elevation. This is because most lower values were calculated from $(La/Yb)_N$, which has a low resolution when the calculated elevation is lower than 3,000 m (Figures 1 and S4). The uncertainly of our calculation ranges from 300 to 1,500 m, with an average of ~900 m (Table S7).

3.2.1. Early Cretaceous

All terranes in Tibet were located at relatively low elevation (≤2,000 m) prior to the Cretaceous (Figures 3 and 4). During the Early Cretaceous, the Southern Qiangtang and Northern Lhasa terranes were uplifted from ~2,000 to 3,000 m (Figure 3). At the same time, the paleo-elevation of the Southern Lhasa terrane (Gangdese arc) was relatively stable at ~2,500 m (Figure 3).

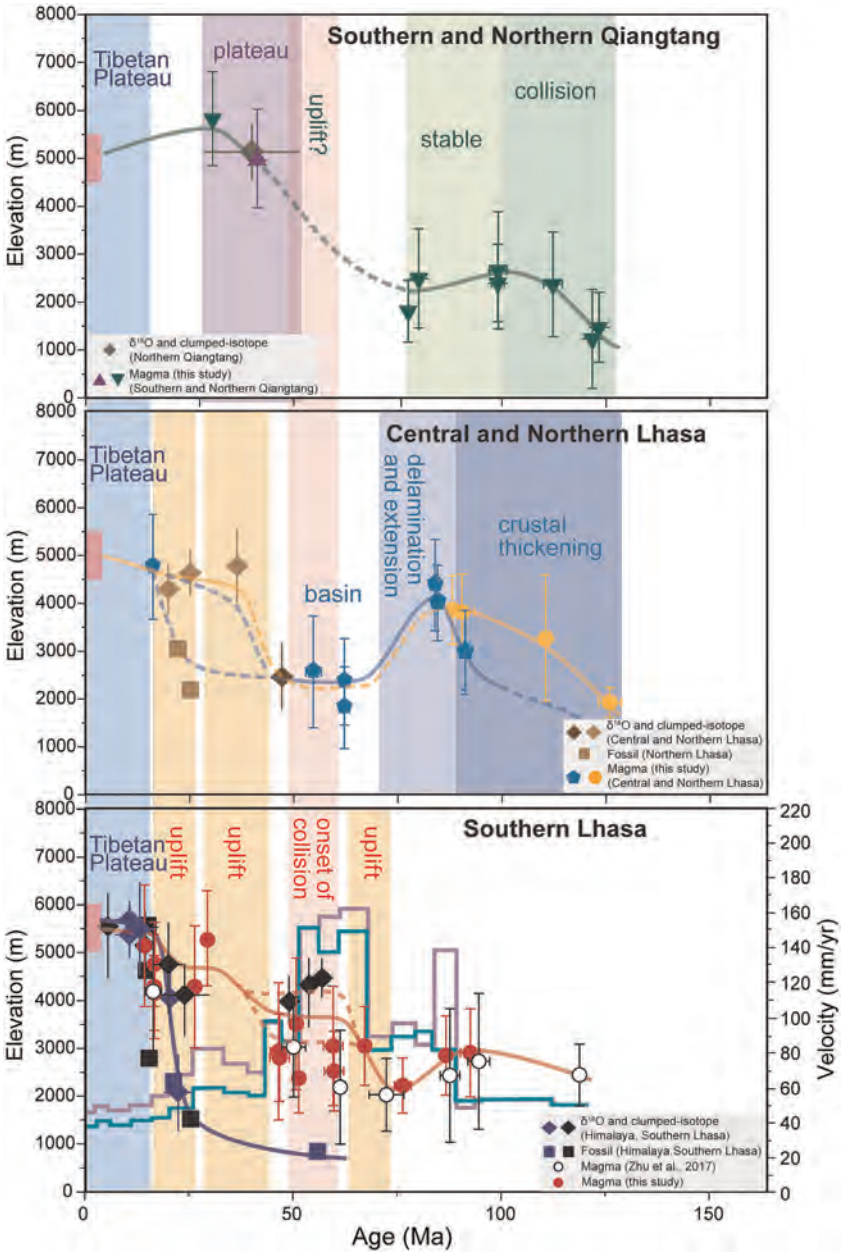

Figure 3. The elevation changes of different terranes of the TP since the Cretaceous (Table S7). Previous published elevation data based on isotopic and fossil studies are also shown for comparison (Table S8). Magmatic data from Zhu et al. (2017) were calculated using equations of this study. The purple and green jagged lines represent relative India-Asia convergence rate at eastern and western Himalayan syntaxis, respectively (after van Hinsbergen et al., 2011).

Our results from the South Qiangtang terrane are consistent with evidence for its fast exhumation during the Early Cretaceous and slow exhumation during ~90–60 Ma (Figure 3; Zhao et al., 2017, 2020). We interpret uplift of the Southern Qiangtang terrane to be related to the collision between the Qiangtang and Lhasa terranes along the Bangong-Nujiang suture in the Early Cretaceous (Kapp, DeCelles, Gehrels, et al., 2007; Lai, Hu, Garzanti, Xu, et al., 2019; Zhao et al., 2020). The low elevations in the Northern and Central Lhasa terranes during the initial collision period are consistent with the contemporaneous carbonate deposition (Lai, Hu, Garzanti, Xu, et al., 2019). As collision continued, the elevation of the Northern Lhasa terrane increased to ~3,000 m during the Early Cretaceous (Figures 3 and 4). No change in the elevation of the Southern Lhasa terrane during the Early Cretaceous is consistent with the fore-arc sedimentary records and a constant convergence rate between India and Asia (Figure 3; Wang et al., 2020).

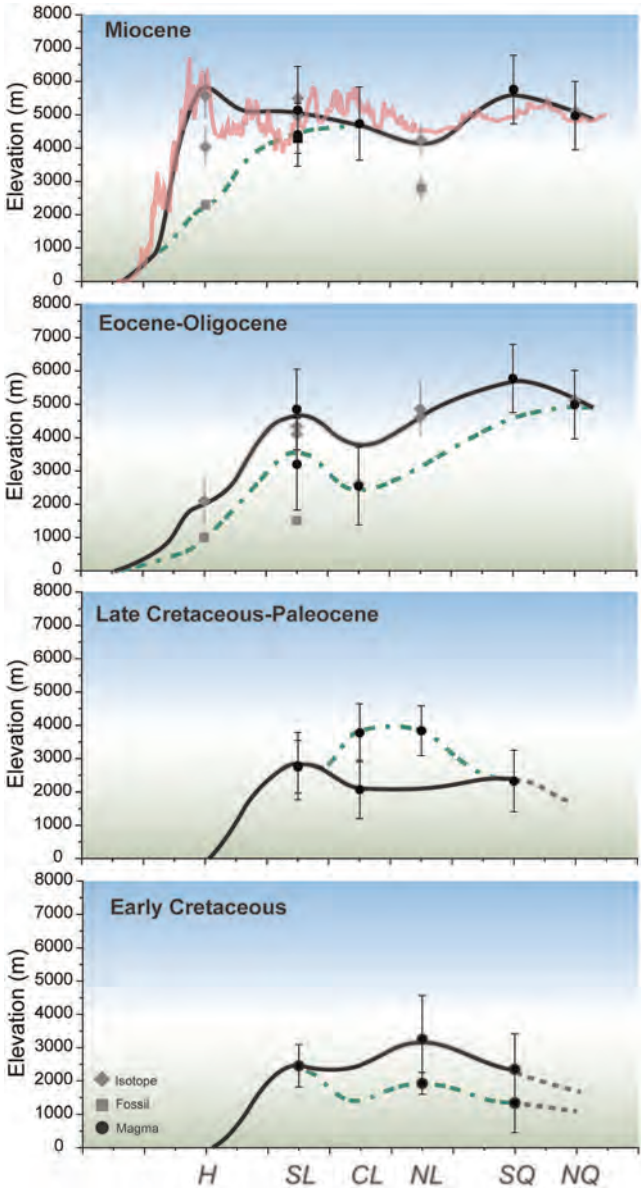

Figure 4. Proposed topography profile representing north (right) to south (left) transects of the TP from the Cretaceous to Miocene (Table S9). The transect location is illustrated as AA′ in Figure 2. The green dashed line represents the paleo-elevation during the middle Early Cretaceous, Late Cretaceous, Eocene, and early Miocene from bottom to top. The black solid line represents the paleo-elevation during the late Early Cretaceous, Paleocene, Oligocene, and late Miocene from bottom to top. The pink line represents the present elevation profile of the TP (AA′ in Figure 1).

3.2.2. Late Cretaceous

During the early Late Cretaceous, the Northern Lhasa and Central Lhasa terranes increased in elevation to ~4,000 m (Figure 3). Based on these results, we interpret the existence of a protoplateau (>3,000 m; the Northern Lhasaplano) in central Tibet during the Late Cretaceous, which exceeded the elevation of the Southern Qiangtang terrane (Figure 4). Opposite to the Central and Northern Lhasa terranes, the paleo-elevation of the Southern Lhasa terrane (Gangdese arc) decreased to ~2,000 m at circa 75 Ma (Figure 3).

Earlier uplift of the Northern Lhasa terrane relative to the Central Lhasa terrane is corroborated by sedimentological studies (DeCelles et al., 2007; Kapp, DeCelles, Gehrels, et al., 2007; Lai, Hu, Garzanti, Sun, et al., 2019), and paleocurrent data support a higher elevation of the Lhasa terrane relative to the Qiangtang terrane during this stage (Figure 4; Lai, Hu, Garzanti, Sun, et al., 2019). High-pressure adakitic rocks derived from the lower crust also support thickened crust during the early Late Cretaceous (Sun, Hu, et al., 2015; Yi et al., 2018). Tectonic shortening/thrusting indicates the upper crust was thickened significantly during the Late Cretaceous (DeCelles et al., 2007; Kapp, DeCelles, Gehrels, et al., 2007), which supports the concept of the Northern Lhasaplano (Figure 4; Lai, Hu, Garzanti, Sun, et al., 2019; Murphy et al., 1997; Wang et al., 2020). The initial uplift of the Gangdese arc during ~96–90 Ma is consistent with increasing input of volcanic rocks from the Gangdese arc to the retro-arc basin (Wang et al., 2020). Acceleration of the convergence rate at ~90 Ma may have also resulted in increased shortening, crustal thickening, and uplift (Figure 3; Li, van Hinsbergen, Shen, et al., 2020). Slab rollback and lower crustal delamination have been proposed for the Gangdese arc (Ji et al., 2014; Zhu et al., 2017), which may explain the subsequent decrease in paleo-elevation observed there and may also lower the elevation in the Central and Northern Lhasa terranes (Figure 3).

3.2.3. Paleocene

The elevation of the Northern Lhasaplano in central Tibet decreased to ~2,500 m at the Paleocene (Figure 3; Xu et al., 2015). Conversely, the Southern Lhasa paleo-elevation increased to ~3,000 m by the start of the Paleogene, which is interpreted to mark the birth of the Lhasaplano. The Southern Lhasa terrane maintained an elevation of ~3,000–3,500 m throughout the Paleocene (Figure 3). Therefore, two protoplateaus were formed successively during the Late Cretaceous to Early Paleogene in the central and southern Tibet, respectively (Figure 4).

The low elevation in central Tibet during this time may be related to pervious postcollisional extension and delamination of the lower crust (Meng et al., 2014; Yi et al., 2018). Increasing elevation in the Southern Lhasa terrane is consistent with evidence for crustal thickening and ongoing subduction (Figure 3; Kapp, DeCelles, Leier, et al., 2007; Zhu et al., 2017). Deformation of the Shexing Formation and unconformities during ~75–65 Ma in the Southern Lhasa documented this crust thickening and uplift process (Leier et al., 2007). The striking increase of the convergence rate at ~70 Ma may also connect to the uplift in the Southern Lhasa (Figure 3; Li, van Hinsbergen, Najman, et al., 2020).

3.2.4. Eocene–Oligocene

During the Eocene to Oligocene, the Qiangtang terrane increased in elevation to ~5,000 m (Figure 3). In contrast, the Southern Lhasa terrane kept an elevation of ~3,000–3,500 m during the Early Eocene and was uplifted significantly during the Late Eocene to Oligocene reaching ~4,000–5,000 m (Figure 3). However, the Central Lhasa terrane and possibly the Northern Lhasa terrane maintained a low elevation of

~2,500 m during the Eocene, which we interpret to represent a paleovalley between high elevations to the north in the Qiangtang terrane and to the south in the Southern Lhasa terrane (Figures 3 and 4).

Uplift of the Qiangtang block is consistent with evidence for major crustal shortening and rapid exhumation (Figure 3; Kapp, DeCelles, Gehrels, et al., 2007; Rohrmann et al., 2012; Wang et al., 2008; Zhao et al., 2020). Magnetic susceptibility analysis of the Gonjo Basin suggests tectonic shortening in the Qiangtang terrane during ~52–48 Ma (Li, van Hinsbergen, Shen, et al., 2020), and oxygen isotopic data suggest that the Qiangtang terrane experienced a significant uplift event during the Eocene to Oligocene (Xu et al., 2013). Our elevation estimates for the Southern Lhasa terrane during the Early Eocene are slightly lower than those from the isotopic studies (~4,000–4,500 m) (e.g., Ding et al., 2014), although they are consistent within uncertainty (Figure 3). The initial India-Asia collision and deceleration of convergence at ~55 Ma should have contributed to crustal deformation (X. Hu et al., 2016; Zheng & Wu, 2018). However, the calculated results show no obvious change of paleo-elevation in the Southern Lhasa terrane, which could be related to a contemporaneous increase in erosion (Ding et al., 2014; Xu et al., 2015). Upper crustal shortening of the Central Lhasa terrane was low during ~50–30 Ma (Kapp, DeCelles, Gehrels, et al., 2007), supporting our interpretation of a paleovalley. Isotopic and paleontological data also support the presence of a paleovalley or intermontane basin (Nima-Lunpola Basin) (Figure 4; Ding et al., 2014; Su et al., 2019). Paleontological and paleoclimatological data show that this valley existed as a topographic feature until the Oligocene (Botsyun et al., 2019; Su et al., 2019; Sun, Wang, et al., 2015), but isotopic data suggest its uplift during the Late Eocene (Rowley & Currie, 2006). The deceleration of convergence at ~45 Ma is proposed to be related to the break-off of the subducted slab (Ji et al., 2016). After this, the long-term low velocity of convergence rate supports a continuous hard collision between India and Asia (van Hinsbergen et al., 2011). Uplift of the Southern Lhasa during the Late Eocene to Oligocene is consistent with rapid exhumation of the Gangdese arc and the activating of the Gangdese thrust belt (~30–23 Ma) (Kapp, DeCelles, Gehrels, et al., 2007; Li et al., 2015; Yin et al., 1999). Late Oligocene to Miocene postcollisional adakitic rocks in southern Tibet also supports thick crust during that time (Chung et al., 2005; Hou et al., 2012).

3.2.5. Miocene

During the Miocene, the convergence rate between India and Asia continued to slow and the Southern Lhasa and Himalaya terranes continued to be uplifted (Figure 3). Underthrusting of India beneath the TP resulted in the expansion of the Himalayan thrust belt and its extraordinarily rapid uplift (Ding et al., 2017; Gébelin et al., 2013; Li et al., 2015). The rise of the Himalaya marked the final formation of the TP (Figure 4; Currie et al., 2005; Rowley & Currie, 2006).

4. Conclusions

Empirically derived equations are presented relating Sr/Y and $(La/Yb)_N$ of intermediate igneous rocks to elevation. These equations can be effectively used to reconstruct the paleo-elevation histories for ancient orogens. Our calculated results for the TP are consistent with results from other paleoaltimetry studies and geological evidence. The Cretaceous amalgamation between the Lhasa and Qiangtang terranes helped to build a protoplateau >3,000 m in elevation in central Tibet, which exceeded the paleo-elevation of the Gangdese arc during the same time. Orogenic collapse reshaped the topography of the central Tibet by the end of the Cretaceous. The TP experienced a differential uplift history during the India-Asia collision. The early uplift of the Qiangtang and Southern Lhasa terranes formed a broad paleovalley in central Tibet during the Eocene before present-day elevations of the whole TP were achieved during the Miocene.

Data Availability Statement

All the data for this research are available online (https://doi.org/10.6084/m9.figshare.12457376.v2) and in the supporting information.

Acknowledgments

F. Y. H. and F. Y. W. acknowledge support from National Natural Science Foundation of China (41888101 and 41902055) and China Postdoctoral Science Foundation (2018M640177). M. N. D. acknowledges support from U.S. National Science Foundation (EAR-1725002) and the Romanian Executive Agency for Higher Education, Research, Development and Innovation Funding project (PN-III-P4-ID-PCCF-2016-0014). The authors declare no conflict of interest. We would like to thank Peter Cawood, Shanying Li, and the Editor Lucy Flesch for their constructive comments and suggestions.

References

Airy, G. B. (1855). On the computation of the effect of the attraction of mountain-masses, as disturbing the apparent astronomical lattitude of stations in geodetic surveys. *Royal Society*, *145*, 101–103. https://doi.org/10.1098/rstl.1855.0003

Alexander, E. W., Wielicki, M. M., Harrison, T. M., DePaolo, D. J., Zhao, Z. D., & Zhu, D. C. (2019). Hf and Nd isotopic constraints on pre- and syn-collisional crustal thickness of southern Tibet. *Journal of Geophysical Research: Solid Earth*, *124*, 11,038–11,054. https://doi.org/10.1029/2019JB017696

Balica, C., Ducea, M. N., Gehrels, G. E., Kirk, J., Roban, R. D., Luffi, P., et al. (2020). A zircon petrochronologic view on granitoids and continental evolution. *Earth and Planetary Science Letters*, *531*, 116005. https://doi.org/10.1016/j.epsl.2019.116005

Bassett, D., Kopp, H., Sutherland, R., Henrys, S., Watts, A. B., Timm, C., et al. (2016). Crustal structure of the Kermadec arc from MANGO seismic refraction profiles: Kermadec Arc Crustal Structure. *Journal of Geophysical Research: Solid Earth*, *121*, 7514–7546. https://doi.org/10.1002/2016JB013194

Botsyun, S., Sepulchre, P., Donnadieu, Y., Risi, C., Licht, A., & Caves Rugenstein, J. K. (2019). Revised paleoaltimetry data show low Tibetan Plateau elevation during the Eocene. *Science*, *363*(6430), eaaq1436. https://doi.org/10.1126/science.aaq1436

Brocher, T. M. (2005). Empirical relations between elastic wavespeeds and density in the Earth's crust. *Bulletin of the Seismological Society of America*, *95*(6), 2081–2092. https://doi.org/10.1785/0120050077

Chapman, J. B., Ducea, M. N., DeCelles, P. G., & Profeta, L. (2015). Tracking changes in crustal thickness during orogenic evolution with Sr/Y: An example from the North American Cordillera. *Geology*, *43*(10), 919–922. https://doi.org/10.1130/g36996.1

Chapman, J. B., Greig, R., & Haxel, G. B. (2020). Geochemical evidence for an orogenic plateau in the southern U.S. and northern Mexican Cordillera during the Laramide orogeny. *Geology*, *48*(2), 164–168. https://doi.org/10.1130/G47117.1

Chapman, J. B., & Kapp, P. (2017). Tibetan magmatism database. *Geochemistry, Geophysics, Geosystems*, *18*, 4229–4234. https://doi.org/10.1002/2017GC007217

Chiaradia, M. (2015). Crustal thickness control on Sr/Y signatures of recent arc magmas: An Earth scale perspective. *Scientific Reports*, *5*(1), 8115. https://doi.org/10.1038/srep08115

Chung, S.-L., Chu, M.-F., Zhang, Y., Xie, Y., Lo, C.-H., Lee, T.-Y., et al. (2005). Tibetan tectonic evolution inferred from spatial and temporal variations in post-collisional magmatism. *Earth-Science Reviews*, *68*(3–4), 173–196. https://doi.org/10.1016/j.earscirev.2004.05.001

Currie, B. S., Rowley, D. B., & Tabor, N. J. (2005). Middle Miocene paleoaltimetry of southern Tibet: Implications for the role of mantle thickening and delamination in the Himalayan orogen. *Geology*, *33*(3), 181–184. https://doi.org/10.1130/g21170.1

DeCelles, P. G., Kapp, P., Ding, L., & Gehrels, G. E. (2007). Late Cretaceous to middle Tertiary basin evolution in the central Tibetan Plateau: Changing environments in response to tectonic partitioning, aridification, and regional elevation gain. *Geological Society of America Bulletin*, *119*(5–6), 654–680. https://doi.org/10.1130/B26074.1

Deng, T., & Ding, L. (2015). Paleoaltimetry reconstructions of the Tibetan Plateau: Progress and contradictions. *National Science Review*, *2*(4), 417–437. https://doi.org/10.1093/nsr/nwv062

Deng, T., Li, Q., Tseng, Z. J., Takeuchi, G. T., Wang, Y., Xie, G., et al. (2012). Locomotive implication of a Pliocene three-toed horse skeleton from Tibet and its paleo-altimetry significance. *Proceedings of the National Academy of Sciences*, *109*(19), 7374–7378. https://doi.org/10.1073/pnas.1201052109

Deng, T., Wang, X., Wu, F., Wang, Y., Li, Q., Wang, S., & Hou, S. (2019). Review: Implications of vertebrate fossils for paleo-elevations of the Tibetan Plateau. *Global and Planetary Change*, *174*, 58–69. https://doi.org/10.1016/j.gloplacha.2019.01.005

Ding, L., Spicer, R. A., Yang, J., Xu, Q., Cai, F., Li, S., et al. (2017). Quantifying the rise of the Himalaya orogen and implications for the South Asian monsoon. *Geology*, *45*(3), 215–218. https://doi.org/10.1130/G38583.1

Ding, L., Xu, Q., Yue, Y., Wang, H., Cai, F., & Li, S. (2014). The Andean-type Gangdese Mountains: Paleoelevation record from the Paleocene–Eocene Linzhou Basin. *Earth and Planetary Science Letters*, *392*, 250–264. https://doi.org/10.1016/j.epsl.2014.01.045

England, P., & Houseman, G. (1989). Extension during continental convergence, with application to the Tibetan Plateau. *Journal of Geophysical Research*, *94*(B12), 17,561–17,579. https://doi.org/10.1029/JB094iB12p17561

Gébelin, A., Mulch, A., Teyssier, C., Jessup, M. J., Law, R. D., & Brunel, M. (2013). The Miocene elevation of Mount Everest. *Geology*, *41*(7), 799–802. https://doi.org/10.1130/G34331.1

He, R., Liu, G., Golos, E., Gao, R., & Zheng, H. (2014). Isostatic gravity anomaly, lithospheric scale density structure of the northern Tibetan Plateau and geodynamic causes for potassic lava eruption in Neogene. *Tectonophysics*, *628*, 218–227. https://doi.org/10.1016/j.tecto.2014.04.047

Hou, Z.-Q., Zheng, Y.-C., Zeng, L.-S., Gao, L.-E., Huang, K.-X., Li, W., et al. (2012). Eocene–Oligocene granitoids in southern Tibet: Constraints on crustal anatexis and tectonic evolution of the Himalayan orogen. *Earth and Planetary Science Letters*, *349-350*, 38–52. https://doi.org/10.1016/j.epsl.2012.06.030

Hu, F., Ducea, M. N., Liu, S., & Chapman, J. B. (2017). Quantifying crustal thickness in continental collisional belts: Global perspective and a geologic application. *Scientific Reports*, *7*(1), 7058. https://doi.org/10.1038/s41598-017-07849-7

Hu, X., Garzanti, E., Wang, J., Huang, W., An, W., & Webb, A. (2016). The timing of India-Asia collision onset—Facts, theories, controversies. *Earth-Science Reviews*, *160*, 264–299. https://doi.org/10.1016/j.earscirev.2016.07.014

Ingalls, M., Rowley, D., Olack, G., Currie, B., Li, S., Schmidt, J., et al. (2018). Paleocene to Pliocene low-latitude, high-elevation basins of southern Tibet: Implications for tectonic models of India-Asia collision, Cenozoic climate, and geochemical weathering. *Geological Society of America Bulletin*, *130*(1–2), 307–330. https://doi.org/10.1130/B31723.1

Ji, W.-Q., Wu, F.-Y., Chung, S.-L., & Liu, C.-Z. (2014). The Gangdese magmatic constraints on a latest Cretaceous lithospheric delamination of the Lhasa terrane, southern Tibet. *Lithos*, *210–211*, 168–180. https://doi.org/10.1016/j.lithos.2014.10.001

Ji, W.-Q., Wu, F.-Y., Chung, S.-L., Wang, X.-C., Liu, C.-Z., Li, Q.-L., et al. (2016). Eocene Neo-Tethyan slab breakoff constrained by 45 Ma oceanic island basalt–type magmatism in southern Tibet. *Geology*, *44*(4), 283–286. https://doi.org/10.1130/G37612.1

Kapp, P., DeCelles, P. G., Gehrels, G. E., Heizler, M., & Ding, L. (2007). Geological records of the Lhasa-Qiangtang and Indo-Asian collisions in the Nima area of central Tibet. *Geological Society of America Bulletin*, *119*(7–8), 917–933. https://doi.org/10.1130/B26033.1

Kapp, P., DeCelles, P. G., Leier, A. L., Fabijanic, J. M., He, S., Pullen, A., et al. (2007). The Gangdese retroarc thrust belt revealed. *GSA Today*, *17*(7), 4. https://doi.org/10.1130/GSAT01707A.1

Lai, W., Hu, X., Garzanti, E., Sun, G., Garzione, C. N., BouDagher-Fadel, M., & Ma, A. (2019). Initial growth of the Northern Lhasaplano, Tibetan Plateau in the early Late Cretaceous (ca. 92 Ma). *Geological Society of America Bulletin*, *131*(11-12), 1823–1836. https://doi.org/10.1130/B35124.1

Lai, W., Hu, X., Garzanti, E., Xu, Y., Ma, A., & Li, W. (2019). Early Cretaceous sedimentary evolution of the northern Lhasa terrane and the timing of initial Lhasa-Qiangtang collision. *Gondwana Research*, *73*, 136–152. https://doi.org/10.1016/j.gr.2019.03.016

Law, R., & Allen, M. B. (2020). Diachronous Tibetan Plateau landscape evolution derived from lava field geomorphology. *Geology*, *48*(3), 263–267. https://doi.org/10.1130/G47196.1

Lee, C.-T. A., Thurner, S., Paterson, S., & Cao, W. (2015). The rise and fall of continental arcs: Interplays between magmatism, uplift, weathering, and climate. *Earth and Planetary Science Letters*, *425*, 105–119. https://doi.org/10.1016/j.epsl.2015.05.045

Leier, A. L., DeCelles, P. G., Kapp, P., & Ding, L. (2007). The Takena Formation of the Lhasa terrane, southern Tibet: The record of a Late Cretaceous retroarc foreland basin. *Geological Society of America Bulletin*, *119*(1–2), 31–48. https://doi.org/10.1130/B25974.1

Li, S., van Hinsbergen, D. J. J., Najman, Y., Liu-Zeng, J., Deng, C., & Zhu, R. (2020). Does pulsed Tibetan deformation correlate with Indian plate motion changes? *Earth and Planetary Science Letters*, *536*, 116,144. https://doi.org/10.1016/j.epsl.2020.116144

Li, S., van Hinsbergen, D. J. J., Shen, Z., Najman, Y., Deng, C., & Zhu, R. (2020). Anisotropy of Magnetic Susceptibility (AMS) analysis of the Gonjo Basin as an independent constraint to date Tibetan shortening pulses. *Geophysical Research Letters*, *47*, e2020GL087531. https://doi.org/10.1029/2020GL087531

Li, Y., Wang, C., Dai, J., Xu, G., Hou, Y., & Li, X. (2015). Propagation of the deformation and growth of the Tibetan–Himalayan orogen: A review. *Earth-Science Reviews*, *143*, 36–61. https://doi.org/10.1016/j.earscirev.2015.01.001

Liu, X., Xu, Q., & Ding, L. (2016). Differential surface uplift: Cenozoic paleoelevation history of the Tibetan Plateau. *Science China Earth Sciences*, *59*(11), 2105–2120. https://doi.org/10.1007/s11430-015-5486-y

McKenzie, N. R., Smye, A. J., Hegde, V. S., & Stockli, D. F. (2018). Continental growth histories revealed by detrital zircon trace elements: A case study from India. *Geology*, *46*(3), 275–278. https://doi.org/10.1130/G39973.1

Meng, F.-Y., Zhao, Z., Zhu, D.-C., Mo, X., Guan, Q., Huang, Y., et al. (2014). Late Cretaceous magmatism in Mamba area, central Lhasa subterrane: Products of back-arc extension of Neo-Tethyan Ocean? *Gondwana Research*, *26*(2), 505–520. https://doi.org/10.1016/j.gr.2013.07.017

Murphy, M. A., Yin, A., Harrison, T. M., Durr, S. B., Ryerson, F. J., & Kidd, W. S. F. (1997). Did the Indo-Asian collision alone create the Tibetan Plateau? *Geology*, *25*(8), 719–722. https://doi.org/10.1130/0091-7613(1997)025<0719:DTIACA>2.3.CO;2

Profeta, L., Ducea, M. N., Chapman, J. B., Paterson, S. R., Gonzales, S. M. H., Kirsch, M., et al. (2015). Quantifying crustal thickness over time in magmatic arcs. *Scientific Reports*, *5*(1), 1, 17786–7. https://doi.org/10.1038/srep17786

Quade, J., Breecker, D. O., Daëron, M., & Eiler, J. (2011). The paleoaltimetry of Tibet: An isotopic perspective. *American Journal of Science*, *311*(2), 77–115. https://doi.org/10.2475/02.2011.01

Rohrmann, A., Kapp, P., Carrapa, B., Reiners, P. W., Guynn, J., Ding, L., & Heizler, M. (2012). Thermochronologic evidence for plateau formation in central Tibet by 45 Ma. *Geology*, *40*(2), 187–190. https://doi.org/10.1130/G32530.1

Rowley, D. B., & Currie, B. S. (2006). Palaeo-altimetry of the late Eocene to Miocene Lunpola basin, central Tibet. *Nature*, *439*(7077), 677–681. https://doi.org/10.1038/nature04506

Rowley, D. B., & Garzione, C. N. (2007). Stable isotope-based paleoaltimetry. *Annual Review of Earth and Planetary Sciences*, *35*(1), 463–508. https://doi.org/10.1146/annurev.earth.35.031306.140155

Searle, M. P., Roberts, N. M. W., Chung, S.-L., Lee, Y.-H., Cook, K. L., Elliott, J. R., et al. (2016). Age and anatomy of the Gongga Shan batholith, eastern Tibetan Plateau, and its relationship to the active Xianshui-he fault. *Geosphere*, *12*(3), 948–970. https://doi.org/10.1130/ges01244.1

Spicer, R. A., Harris, N. B. W., Widdowson, M., Herman, A. B., Guo, S., Valdes, P. J., et al. (2003). Constant elevation of southern Tibet over the past 15 million years. *Nature*, *421*(6923), 622–624. https://doi.org/10.1038/nature01356

Su, T., Farnsworth, A., Spicer, R. A., & Huang, J. (2019). No high Tibetan Plateau until the Neogene. *Science Advances*, *5*(3), eaav2189. https://doi.org/10.1126/sciadv.aav2189

Sun, B., Wang, Y.-F., Li, C.-S., Yang, J., Li, J.-F., Li, Y.-L., et al. (2015). Early Miocene elevation in northern Tibet estimated by palaeobotanical evidence. *Scientific Reports*, *5*(1), 1–6. https://doi.org/10.1038/srep10379

Sun, G.-Y., Hu, X.-M., Zhu, D.-C., Hong, W.-T., Wang, J.-G., & Wang, Q. (2015). Thickened juvenile lower crust-derived ~90Ma adakitic rocks in the central Lhasa terrane, Tibet. *Lithos*, *224–225*, 225–239. https://doi.org/10.1016/j.lithos.2015.03.010

Tapponnier, P., Zhiqin, X., Roger, F., Meyer, B., Arnaud, N., Wittlinger, G., & Jingsui, Y. (2001). Oblique stepwise rise and growth of the Tibet Plateau. *Science*, *294*(5547), 1671–1677. https://doi.org/10.1126/science.105978

Taylor, M., & Yin, A. (2009). Active structures of the Himalayan-Tibetan orogen and their relationships to earthquake distribution, contemporary strain field, and Cenozoic volcanism. *Geosphere*, *5*(3), 199–214. https://doi.org/10.1130/GES00217.1

van Hinsbergen, D. J. J., Steinberger, B., Doubrovine, P. V., & Gassmöller, R. (2011). Acceleration and deceleration of India-Asia convergence since the Cretaceous: Roles of mantle plumes and continental collision. *Journal of Geophysical Research*, *116*, B06101. https://doi.org/10.1029/2010JB008051

Wang, C., Zhao, X., Liu, Z., Lippert, P. C., Graham, S. A., Coe, R. S., et al. (2008). Constraints on the early uplift history of the Tibetan Plateau. *Proceedings of the National Academy of Sciences*, *105*(13), 4987–4992. https://doi.org/10.1073/pnas.0703595105

Wang, J.-G., Hu, X., Garzanti, E., BouDagher-Fadel, M. K., Liu, Z.-C., Li, J., & Wu, F.-Y. (2020). From extension to tectonic inversion: Mid-Cretaceous onset of Andean-type orogeny in the Lhasa block and early topographic growth of Tibet. *Geological Society of America Bulletin*, *n/a*, n/a. https://doi.org/10.1130/B35314.1

Xu, Q., Ding, L., Hetzel, R., Yue, Y., & Rades, E. F. (2015). Low elevation of the northern Lhasa terrane in the Eocene: Implications for relief development in south Tibet. *Terra Nova*, *27*(6), 458–466. https://doi.org/10.1111/ter.12180

Xu, Q., Ding, L., Zhang, L., Cai, F., Lai, Q., Yang, D., & Liu-Zeng, J. (2013). Paleogene high elevations in the Qiangtang Terrane, central Tibetan Plateau. *Earth and Planetary Science Letters*, *362*, 31–42. https://doi.org/10.1016/j.epsl.2012.11.058

Yi, J.-K., Wang, Q., Zhu, D.-C., Li, S.-M., Liu, S.-A., Wang, R., et al. (2018). Westward-younging high-Mg adakitic magmatism in central Tibet: Record of a westward-migrating lithospheric foundering beneath the Lhasa–Qiangtang collision zone during the Late Cretaceous. *Lithos*, *316-317*, 92–103. https://doi.org/10.1016/j.lithos.2018.07.001

Yin, A., Harrison, T. M., Murphy, M. A., Grove, M., Nie, S., Ryerson, F. J., et al. (1999). Tertiary deformation history of southeastern and southwestern Tibet during the Indo-Asian collision. *Geological Society of America Bulletin*, *111*(11), 1644–1664. https://doi.org/10.1130/0016-7606(1999)111%3C1644:TDHOSA%3E2.3.CO;2

Zhao, Z., Bons, P. D., Li, C., Wang, G. H., Ma, X. X., & Li, G. W. (2020). The Cretaceous crustal shortening and thickening of the South Qiangtang Terrane and implications for proto-Tibetan Plateau formation. *Gondwana Research*, *78*, 141–155. https://doi.org/10.1016/j.gr.2019.09.003

Zhao, Z., Bons, P. D., Stübner, K., Wang, G.-H., & Ehlers, T. A. (2017). Early Cretaceous exhumation of the Qiangtang Terrane during collision with the Lhasa Terrane, Central Tibet. *Terra Nova*, *29*(6), 382–391. https://doi.org/10.1111/ter.12298

Zheng, Y., & Wu, F. (2018). The timing of continental collision between India and Asia. *Science Bulletin*, *63*(24), 1649–1654. https://doi.org/10.1016/j.scib.2018.11.022

Zhu, D.-C., Wang, Q., Cawood, P. A., Zhao, Z.-D., & Mo, X.-X. (2017). Raising the Gangdese Mountains in southern Tibet. *Journal of Geophysical Research: Solid Earth*, *122*, 214–223. https://doi.org/10.1002/2016JB013508

Zhu, D.-C., Wang, Q., Chung, S.-L., Cawood, P. A., & Zhao, Z.-D. (2019). Gangdese magmatism in southern Tibet and India–Asia convergence since 120 Ma. *Geological Society, London, Special Publications*, *483*(1), 583–604. https://doi.org/10.1144/SP483.14